Exploring How to Increase the Brightness of Surface-Enhanced Raman Spectroscopy Nanolabels: The Effect of the Raman-Active Molecules and of the Label Size

Vincenzo Amendola and Moreno Meneghetti**

Due to the surface-enhanced Raman scattering (SERS) effect, SERS labels based on noble-metal nanoparticles loaded with Raman-active molecules are good candidates for ultrasensitive multiplexed assays and in vitro/in vivo imaging. However, understanding how to maximize the brightness of such labels is of paramount importance for their widespread application. The effective differential Raman scattering cross-section ($d\sigma_R/d\Omega$) of SERS labels made of pegylated gold nanoparticles loaded with various Raman active molecules (Raman reporters) is studied. It is found that proper choice of the Raman reporter and of nanoparticle size can enhance the $d\sigma_R/d\Omega$ by several orders of magnitude. The experimental results are understood by considering the molecular cross-section for resonant Raman scattering and the local electromagnetic enhancement factor (G_{SERS}) in the nearby of gold nanoparticles. These results are useful to guide the design of SERS labels with improved performances and to provide a reference for the comparison of the absolute value of the $d\sigma_R/d\Omega$ of SERS labels based on metal nanoparticles.

1. Introduction

New physical phenomena of great interest for basic science and for technological applications are observed in metal nanoparticles, such as the surface-enhanced Raman scattering (SERS) effect.[1,2] Normally, Raman scattering is weak compared to Raleigh scattering or fluorescence, but when Raman-active molecules are adsorbed on the surface of metallic nanostructures with plasmonic properties, SERS enhances the molecular Raman scattering cross-section by up to a factor of 10^{14}.[1,3–5] Theory and experiments have evidenced that SERS principally originates from the enhancement of the local electromagnetic field on the surface of plasmonic nanostructures (electromagnetic enhancement) and, to a minor extent, also from charge-transfer processes between the molecule and the metal substrate (chemical enhancement).[1,3,6] Further amplification of the Raman signals is possible when the Raman-active molecules (Raman reporters) are in resonance with the laser excitation wavelength and suffer strong fluorescence quenching due to their proximity to the metal surface. This latter case is called surface-enhanced resonant Raman scattering (SERRS).[1,3]

The signals originating from SERS are so intense that they can be exploited for labelling.[7–19] SERS labels usually consist of plasmonic nanoparticles that have Raman reporters anchored to their surface, are coated with a protecting/stabilizing external layer, and are equipped with a targeting function for the selective binding of analytes like DNA, proteins, or antigens on cell membranes.[7–19] SERS labels have several peculiarities when compared to organic fluorophores or semiconductor quantum dots: i) the bandwidth of Raman peaks is one order of magnitude smaller than fluorescence emission bands;[20–22] ii) each Raman reporter has a distinctive vibrational fingerprint and multiple Raman reporters can be combined on a single SERS label to give multiple distinctive spectral signatures;[20,21] iii) multiple SERS labels can be excited with the same excitation wavelength;[21,23] iv) SERS labels do not suffer from photobleaching and basically no blinking is observed for acquisition times of seconds;[7,24] v) background interference in Raman measurements can be avoided by excitation with red or near-infrared laser lines, while many florescent labels can suffer from autofluorescence background, especially if they require visible-light excitation;[7,21] vi) the excitation wavelength can be shifted to the red or near-infrared, where the tissue penetration depth is greater and where there is a limited number of bright fluorescent labels;[7,22] vii) bioconjugation techniques for noble-metal nanoparticles are well consolidated and can be used to confer high selectivity onto SERS labels;[7,21,24] viii) gold nanostructures are biocompatible, in contrast with the cytotoxicity of ordinary semiconductor quantum dots.[24,25] Due to these peculiarities, SERS labels are very attractive for multiplexed analysis and in vivo labelling.

To date, several types of SERS labels have been used for bioanalytical applications or in vitro/in vivo imaging, like isolated or aggregated gold and silver nanoparticles, Au–Ag core-shell nanoparticles, nanorods, nanoflowers, nanostars, and nanocages.[7,8,10,13,15,18,19,26–32] Some of them also have the potential for photothermal therapy in the near-infrared spectral window.[9,22,32–35] Despite the wide variety of SERS labels that has been developed, no information is currently available to quantitatively evaluate which type of label delivers the best performance

Prof. V. Amendola, Prof. M. Meneghetti
Department of Chemical Sciences
University of Padova
Via Marzolo 1, I-35131 Padova, Italy
E-mail: vincenzo.amendola@unipd.it;
moreno.meneghetti@unipd.it

DOI: 10.1002/adfm.201101539

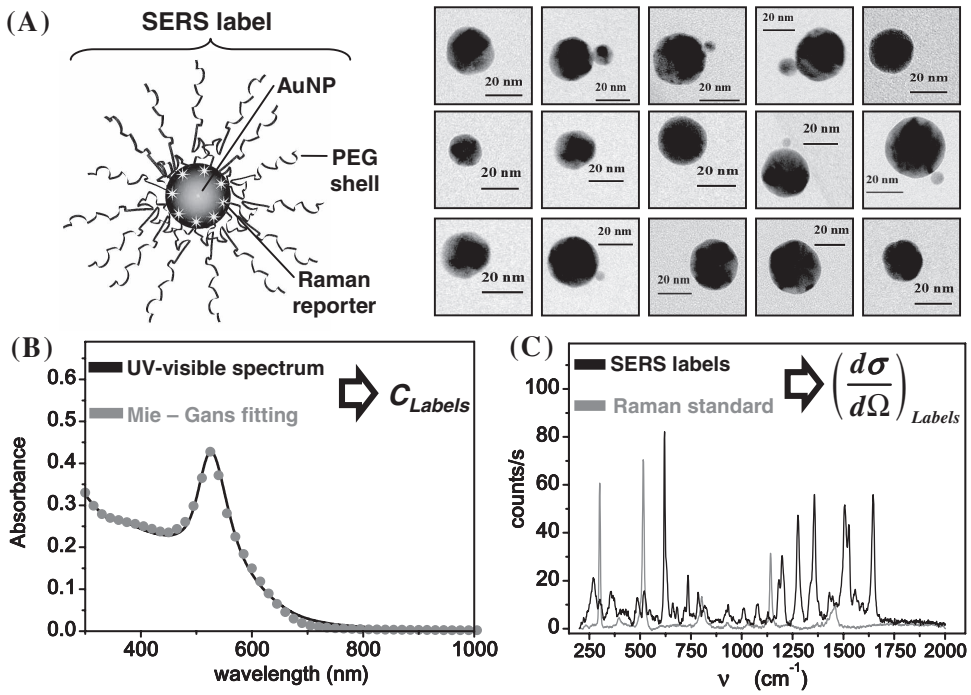

Figure 1. The procedure for the determination of the effective $d\sigma_R/d\Omega$ of the SERS labels is summarized here, using as an example the R6G SERS labels. A) Left: Sketch of the structure of SERS labels. Right: TEM images representative of the R6G SERS labels. B) The MG fitting (gray dots) of the UV–vis spectrum of the solution of R6G labels (black line) was used to determine the label concentration. C) The most intense band in the Raman spectrum of R6G labels (at 620 cm^{-1}) was fitted with a Lorentzian curve and its intensity was compared to that of the reference bands of two Raman standards. The spectrum of one of these standard, 2B2MP, is also reported in gray in the graph.

for a given application and what parameters should be considered to design the SERS label with the highest brightness. Also, when single-label studies have been reported, like Raman spectroscopy in the dark-field configuration,[7,12,22] this type of investigation did not allow an absolute comparison of different SERS labels. This is a strong limitation for the improvement of label brightness and for their widespread application,[11,21,36,37] and one possible reason is that many studies have focused on the enhancement factor in the hot spots as a benchmark for the comparison of different nanostructures for SERS. However, in the application of SERS nanostructures for labeling, the relevant parameter is the brightness of the whole label. The brightness is proportional to the amount of Raman-scattered photons over the total of the incident photons and, therefore, it depends on the Raman-scattering cross-section of the whole label.

Here we report the study of the effective differential Raman-scattering cross-section ($d\sigma_R/d\Omega$) of SERS nanolabels based on pegylated gold nanoparticles. Two fundamental parameters were evaluated quantitatively; the type of the Raman reporter and the size of nanoparticles. The experimental results were interpreted by referring to the molecular expression for the resonant Raman-scattering cross-section and by accounting for the SERS electromagnetic enhancement factor G_{SERS} based on calculations of the local electric field with the discrete-dipole approximation (DDA) method. Our results show that the above parameters account for a variation of the Raman cross-section of several orders of magnitude and, therefore, provide useful indications for the design of SERS labels with improved performances.

2. Experimental Results

Our SERS labels consist of pegylated AuNPs loaded with 12 different types of Raman reporter molecules (**Figure 1**a). These molecules are pyridine (PYR) and 11 cationic dyes: methylene blue (BM), cresyl violet 670 (CV), hexacyanin 3 (HITC), styryl 13 (LDS), malachite green (MG), malachite green isothiocyanate (MGITC), nile blue A (NB), oxazine 750 (OX), rhodamine 6G (R6G), rhodamine B (RB), and tetramethylrhodamine isothiocyanate (TRITC). We used AuNPs obtained by LASiS in NaCl solution, which possess a negative charge due to the reaction of a small fraction of surface Au atoms (about 6%) with O and Cl atoms.[38,39] The cationic dyes absorb onto negatively charged particles by means of electrostatic interactions. Different from the cationic dyes, pyridine is well known to adsorb on bare gold surfaces through a physical bond.[40,41] After the absorption of the Raman reporters, AuNPs were coated with a stabilizing layer of thiolated PEG. The PEG shell has the function of conferring solubility in aqueous solution, stability in physiological medium, and stealth character in biological environments to the SERS label and, eventually, it can provide the external functional groups required for the bioconjugation of the SERS labels with a targeting moiety.[7]

All the Raman reporters were added in large excess (10000:1) to AuNP solutions and the unbound molecules were removed by centrifugation after 14 hours of incubation. No traces of the Raman reporters were detected by UV–visible spectroscopy in the final SERS label solutions. This finding suggests that less

than 100–200 molecules are adsorbed for each AuNP in all of our SERS labels, as previously reported.[42] Some representative TEM images for the labels are displayed in Figure 1a, showing that they predominantly consist of isolated AuNPs and small AuNP dimers made of two nanoparticles of different size.

The concentration of SERS labels in each solution was evaluated by the Mie–Gans fitting of their UV–vis spectrum (an example is reported in Figure 1b and the fitting parameters for all samples are reported in Table S1 in the Supporting Information). The same solutions were used for recording the Raman spectra, exciting at 632.8 nm. The strongest Raman band in each spectra was fitted with a Lorentzian curve, and the corresponding $d\sigma_R/d\Omega$ value was obtained by comparison with the Raman bands of the two standards (an example is reported in Figure 1c, for details see the Experimental Section) and by accounting for the number of labels in solution. In the cases of AuNPs loaded with BM, NB, and OX two well-defined Raman bands dominate the spectrum (Figure S2 in the Supporting Information) and the value of $d\sigma_R/d\Omega$ was calculated for both bands. The values of $d\sigma_R/d\Omega$ calculated by this method are the average of all the SERS labels in solution. As shown in **Figure 2**, we measured $d\sigma_R/d\Omega$ to be of the order of 10^{-20} cm^2 sr^{-1} for the single nanolabel. The highest value was obtained for AuNPs loaded with malachite green, with $d\sigma_R/d\Omega = 7.6 \pm 1.4\ 10^{-20}$ cm^2 sr^{-1}. A two order of magnitude smaller value is observed for the less-bright SERS labels that are AuNPs loaded with pyridine. These values are lower than the photoluminescence cross-section of organic dyes or semiconductor quantum dots, which are of the order of 10^{-18}–10^{-17} cm^2 sr^{-1} and 10^{-17}–10^{-16} cm^2 sr^{-1} respectively.[43] However, the direct comparison of the Raman cross-section of SERS labels with the photoluminescence cross-section of fluorophores is not straightforward, because the signal-to-noise ratio of Raman measurements is generally larger, due to the small bandwidth and to the low background, especially with red or near-infrared excitation, and it can be sensibly increased by using longer integration times due to the absence of photobleaching or blinking.[19,21,24] In any case, these figures suggest that maximizing the brightness of SERS labels is important for their widespread application.

The intensity of the Raman-scattering cross-section was evaluated also as a function of AuNP size d. We prepared SERS labels with the same Raman reporter but different nanoparticle size by centrifugation at different relative centrifugal forces and the Raman-scattering cross-section was evaluated for each of these preparations. The average size and the percentage of aggregates for all the AuNPs solutions was evaluated by using the Mie–Gans fitting and confirmed by means of transmission electron microscopy (TEM) analysis of selected samples. The results showed that we obtained AuNPs with average sizes in the 10–23 nm range and that the fraction of nonspherical AuNPs remained almost unchanged, independent of the average AuNP size (fitting parameters are reported in Table S2 in the Supporting Information). In **Figure 3** we plot the $d\sigma_R/d\Omega$ value for OX, MG, CV, and NB as a function of label size. $d\sigma_R/d\Omega$ was rescaled to the value of the sample with a size of ca. 17 nm, to include all the experimental data of the four different labels in a single plot. A strong dependence of the $d\sigma_R/d\Omega$ value on the average size of the labels is evident from Figure 3 and all labels show the same trend. The dependence of the normalized $d\sigma_R/d\Omega$ versus d is well fitted by a power law with an exponent of 4.2 ± 0.2 (black line in Figure 3).

3. Discussion

We can express the $d\sigma_R/d\Omega$ value of a SERS label as the sum of the Raman-scattering cross-section of all the Raman reporter molecules hosted in the label as Equation 1:

$$\left(\frac{d\sigma_R}{d\Omega}\right)_{Label} = \sum_i^{N_{Rr}} G^i_{SERS} F^i_{Rr} = F_{Rr} \sum_i^{N_{Rr}} G^i_{SERS} \quad (1)$$

N_{Rr} is the total number of Raman reporters in the single label and can be considered proportional to the surface area of gold nanoparticles, i.e., N_{Rr} is proportional to d^2. F_{Rr} is the term that

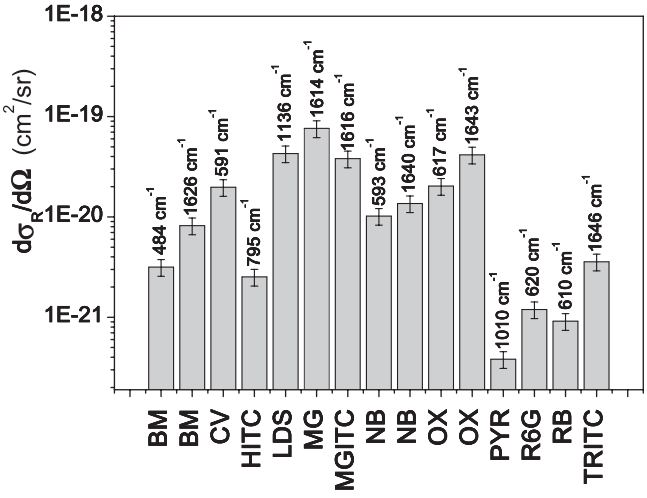

Figure 2. The differential Raman-scattering cross-section ($d\sigma_R/d\Omega$) for excitation at 632.8 nm measured for the most intense bands of the 12 SERS labels. The wavenumber corresponding to the Raman band is reported above each bar.

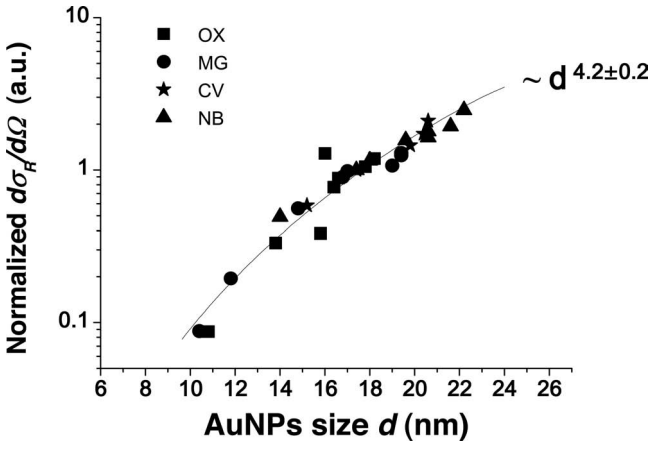

Figure 3. The normalized $d\sigma_R/d\Omega$ value versus average AuNP size for MG (circles), CV (stars), OX (squares), and NB (triangles) labels. In all cases, the normalized values of $d\sigma_R/d\Omega$ show a power-law dependence on the average AuNPs size as $d^{4.2 \pm 0.2}$.

depends on the Raman-scattering cross-section of the Raman reporter. G_{SERS} is the SERS enhancement factor and it accounts for the actual local electric field E_{loc} that is probed by each molecule on the surface of the metal nanoparticle during the Raman measurement, therefore it depends on the structure of the nanoparticle and on the localization of the Raman reporter. From Equation (1) it is clear that the performances of the SERS labels can not be compared only by looking at the enhancement factor and one must consider also the Raman-scattering cross-section of the single Raman reporters and the summation over all the Raman reporters hosted in the label. In particular, the $d\sigma_R/d\Omega$ value of ordinary organic molecules is of the order of 10^{-32}–10^{-30} cm^2 sr^{-1}, but it can be as high as 10^{-24} cm^2 sr^{-1} in the case of resonant Raman scattering.[44] Some of the Raman reporter molecules are dyes with electronic transitions close to the 632.8 nm excitation wavelength. The single-molecule Raman-scattering cross-section depends on the molecule polarizability tensor,[45,46] and in close to resonance conditions the only relevant contributions are those corresponding to the transition from the ground to the excited electronic state. Therefore, for a vibrational mode with energy ω_{fi}, we can express F_{Rr} by the following simplified expression:[45–48]

$$F_{Rr} \approx K \frac{(\omega_L - \omega_{fi})^4 / \omega_{fi}}{\left[1 - \exp(-\hbar\omega_{fi}/k_B T)\right]} \frac{|\langle f|v'\rangle \langle v'|i\rangle|^2}{(\omega_{ge} - \omega_L)^2 + \Gamma^2} \quad (2)$$

where ω_L is the frequency of the incoming excitation photons; ω_{ge} is the frequency of the transition from the vibrational state i of the ground electronic state g to the vibrational state v' of the excited electronic state e; f is the final vibrational state of the inelastic scattering process; $\langle f|v'\rangle$ and $\langle v'|i\rangle$ are the Franck–Condon overlap amplitudes; Γ is the damping term of the electronic transition; k_B is the Boltzmann constant; T is the temperature and K contains all the other constant terms. It is worth pointing out that the second term of Equation 2 is a Lorentzian with a maximum where the laser excitation wavelength equals the electronic resonance. In **Figure 4**, we show

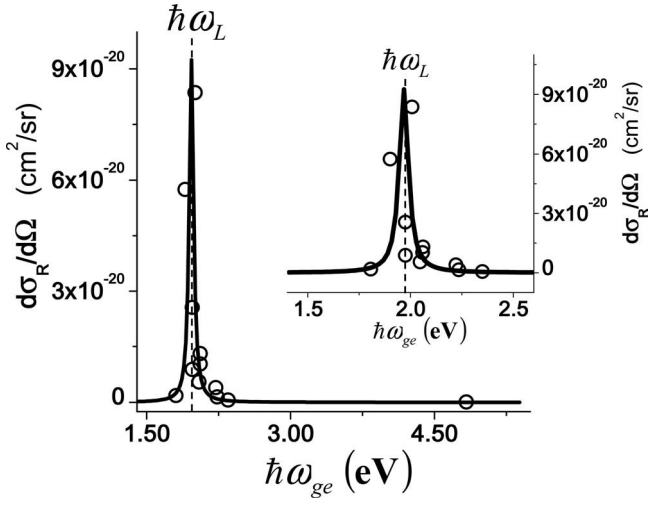

Figure 4. Values of $d\sigma_R/d\Omega$ versus the optical excitation energy $\hbar\omega_{ge}$ of the 12 SERS labels (circles) is well fitted by a Lorentzian curve (black line) centered at the laser excitation energy $\hbar\omega_L$ of 1.96 eV (632.8 nm). Inset shows a magnification of the region around the Lorentzian maximum.

that the experimental values of $d\sigma_R/d\Omega$ plotted as a function of ω_{ge} for the 12 Raman reporters are well fitted by a Lorentzian cruve with ω_L set at 632.8 nm. Deviations from the Lorentzian fit can be due to slight differences in ω_{fi}, Γ, and the Franck–Condon factor for the 12 different Raman reporters. One should consider also that different dyes can have different surface coverage on the AuNPs, although our experimental procedure should help in minimizing these differences (for details see Experimental Section). In any case, Figure 4 points out that the brightness of the SERS labels can be increased by one to two orders of magnitude simply by using Raman reporters that are resonant at the excitation wavelength.

The data reported in Figure 3 evidence, instead, the dependence from a structural parameter like the average size d of gold nanoparticles. In Equation (1), the dependence on the structure of the nanoparticles is present in the G_{SERS} term. A complete calculation of the SERS enhancement for a monolayer of molecules on the surface of a metal nanoparticle, as required by Equation (1), is a complicated problem. Le Ru et al. theoretically solved the problem for the special case of a dimer composed of two identical metal nanoparticles.[49] The theoretical solution was confirmed experimentally by the same authors[50] and by Dlott et al.[51] They demonstrated that the distribution of enhancement factors $p(G_{SERS})$ for metal nanoparticles in the presence of a collection of hot spots with different geometrical parameters has a long tail nature that can be well described according to the following analytical expression:[52]

$$p(G_{SERS}) = AG_{SERS}^{-(1+k)} \exp\left[(G_{SERSS}/G_{SERS}^{H})^{\eta}\right] \quad (3)$$

where A, k, and η are phenomenological parameters of the system that do not vary much for different systems and $G_{SERS}{}^{H}$ is related to the maximum enhancement of the collection of hot spots. Equation 3 is the product of a truncated Pareto distribution with a stretched exponential and it is a direct consequence of the fact that the contributions of the points far from the hot spots are negligible.[49,52] In case of systems with just one type of hot spots, the exponential term becomes 1 and equation (3) reduces to the truncated Pareto distribution of Equation 4:[49,52]

$$p(G_{SERS}) = AG_{SERS}^{-(1+k)} \text{ for } G_{SERS} < G_{SERS}^{MAX} \quad (4)$$

where G_{SERS}^{MAX} is the maximum enhancement factor of the system. In this case, the average enhancement factor $\langle G_{SERS}\rangle$ over the surface of the nanoparticle can be analytically evaluated[49] as Equation 5:

$$\langle G_{SERS}\rangle = \frac{A}{1-k}(G_{SERS}^{MAX})^{1-k} \quad (5)$$

Since the term $1–k$ is ~1 (k is ca. 0.1), independent of nanoparticle size and composition and of interparticle gap, the average enhancement on the surface of a nanoparticle dimer is roughly proportional to the maximum enhancement G_{SERS}^{MAX}.[49] Le Ru et al. speculated that the trend described by Equation 4 for a dimer is qualitatively and semiquantitatively still valid also for different nanostructures, provided that a single type of hot spot is present.[49] This assumption is especially true when nanostructures of the same type and composition are compared (for instance, dimers with dimers, trimers with trimers etc.).

If we express the Raman-scattering cross-section of Equation 1 as a function of the average enhancement factor, as in Equation 6:

$$\left(\frac{d\sigma_R}{d\Omega}\right)_{Label} = F_{Rr}\sum_{i}^{N_{Rr}} G^{i}_{SERS} = F_{Rr}\,N_{Rr}\,\langle G_{SERS}\rangle \quad (6)$$

we can see that the dependence of $d\sigma_R/d\Omega$ on the AuNP size d is contained in N_{Rr} and in $\langle G_{SERS}\rangle$. The calculations of Le Ru, Etchegoin et al. suggest that we can obtain indications about the dependence of $\langle G_{SERS}\rangle$ on d by looking at the dependence of G^{MAX}_{SERS} on d. As a first approximation, G_{SERS} can be considered similar to the fourth power of the ratio between the E_{loc} probed by the Raman reporters and the incident field E_0.[53,54] We used finite element calculations with the DDA method to evaluate the distribution of the G_{SERS} on the surface of AuNPs. We calculated $G_{SERS} = (|E_{loc}|/|E_0|)^4$ in the proximity of spherical AuNPs with sizes in the 5–35 nm range, when excited by linearly polarized electromagnetic radiation at 632.8 nm. In **Figure 5**a we give three examples of the G_{SERS} distribution for spherical AuNPs (graphs I, II, III), which show that G_{SERS} of the order of 10^2 are measured only in a limited portion of the area near the particle surface. This result is in agreement with the results of Equation 5, namely that the prevailing contributions to the summation of Equation (1) will be from Raman reporters in the proximity of the region with the highest G_{SERS} value. The log plot of G^{MAX}_{SERS} at a distance of 0.5 nm from the surface of the AuNPs (indicated by the yellow arrow in Figure 5a) showed a dependence on d with an exponent of 0.40 ± 0.01 (black line in Figure 5b). By accounting also for N_{Rr}~d^2, we estimate an overall dependence of $d\sigma_R/d\Omega$ on $d^{2.4}$. The experimental data of Figure 3 showed a dependence on $d^{4.2}$, meaning that other contributions to $d\sigma_R/d\Omega$ must be considered. In particular, the MG fitting of UV–vis spectra clearly evidenced the presence of approximately 20%–40% nonspherical nanoparticles and the TEM analysis showed that these nonspherical nanoparticles are AuNP heterodimers (Figure 1a). According to experimental and theoretical calculations, the value of G_{SERS} can be as high as of 10^3–10^8 in the hot spots at the junction between two spherical AuNPs, like in small aggregates.[40,54–63] Therefore, G_{SERS} calculations were performed also on i) heterodimers composed by a first AuNP of 5 nm and a second nanoparticle with size varied in the 5–30 nm range and ii) homodimers composed by two identical AuNPs with size varied in the 5–30 nm range (all the plot of G_{SERS} are shown in Figure S3).

By using local field calculations in AuNP heterodimers (Figure 5a and S3), we found G^{MAX}_{SERS} values of 10^4–10^5, namely two to three orders of magnitude larger than for isolated spherical AuNPs. The plot of G^{MAX}_{SERS} versus the effective dimer size d_{eff}, defined as $d_{eff} = (3V_{dimer}/4\pi)^{1/3}$ where V_{dimer} is the dimer volume, revealed a dependence on the 2.6^{th} ± 0.1 power of d_{eff} (red circles in Figure 5b). When accounting also for the dependence of the number of molecules on d^2, we estimate an overall dependence of $d\sigma_R/d\Omega$ on $d^{4.6}$, which is close to the experimental value of $d^{4.2}$. This result indicates that the Raman reporters in the hot spots of AuNPs heterodimers dominate the summation in Equation 1.

Interestingly, in the case of homodimers, the G^{MAX}_{SERS} in the hot spots reach values of the order of 10^5–10^8, which is much higher than in heterodimers. The observation of larger enhancements at the hot spots of homodimers than of heterodimers is in agreement with what has previously been reported about silver nanoparticles.[64,65] In homodimers, we found that G^{MAX}_{SERS} depends on the 6.9^{th} ± 0.8 power of the effective dimer size d_{eff} (green line in Figure 5b), which is far from what we observed experimentally. On the other hand, homodimers were not evidenced in TEM analysis of our samples.

4. Conclusions

In summary, we quantitatively studied the $d\sigma_R/d\Omega$ values of SERS nanolabels based on pegylated AuNPs loaded with different Raman reporters. The experimental results pointed out that the brightness of SERS labels can be increased of several orders of magnitude by using resonant Raman reporters. Moreover, the experimental data show the existence of a power-law dependence of $d\sigma_R/d\Omega$ on the size of AuNPs. By using DDA calculations of the local electric field, we found that the experimental results can be explained by the strong dependence of the SERS enhancement factor G_{SERS} on the AuNP size and by the presence of hot spots in the AuNP heterodimers. Moreover, DDA calculations suggest that hot spots in homodimers can provide the highest value of G_{SERS} and the strongest dependence on the AuNPs size. These results are useful in guiding the development of SERS labels with improved performances, which is a stringent requirement for their widespread application in ultrasensitive multiplex labeling and in vitro/in vivo imaging.

5. Experimental Section

Synthesis of SERS Labels: We obtained SERS labels based on pegylated AuNPs by a procedure similar to that previously reported.[42] We used AuNPs obtained by laser ablation synthesis in solution (LASiS). AuNPs with average size of 19 nm were obtained by 9-ns laser pulses at 1064 nm (from a Nd:YAG Quantel YG981E laser) focused with a 10-cm focus lens on a 99.99% pure gold plate placed at the bottom of a cell containing a 10^{-5} M NaCl solution in double-distilled water.[38,42] Pulses with fluence of 10 J cm^{-2} at 10 Hz repetition rate for 60 minutes were employed.

Freshly prepared Raman active dyes solutions (1 mM in ethanol) were added to a 2 nM AuNP solution in a 1:50 volume ratio. The following dyes were used: methylene blue (BM, trihydrate, Sigma-Aldrich); cresyl violet 670 (CV, Perchlorate, Exciton); hexacyanin 3 (HITC, Perchlorate, Exciton); styryl 13 (LDS925, Perchlorate, Exciton); malachite green (MG, oxalate salt, Sigma-Aldrich); malachite green isothiocyanate (MGITC, Invitrogen); nile blue A (NB, sulfate, Sigma-Aldrich); oxazine 750 (OX, perchlorate, Exciton); pyridine (PYR, Sigma-Aldrich); rhodamine 6G (R6G, chloride, Exciton); rhodamine B (RB, chloride, Sigma-Aldrich); and tetramethylrhodamine isothiocyanate (TRITC, mixed isomers, Sigma-Aldrich). After 30 minutes under mild stirring, a freshly prepared aqueous solution of thiolated poly(ethylene glycol) (PEG, MW 5000, Lysan Bio) was added to the AuNPs in a ratio of 15000 PEG molecules to each nanoparticle. The mixtures were maintained under mild stirring for 14 hours at room temperature. After incubation, the suspensions were washed several times by centrifugation at 3000 rcf for 10 minutes. At the end of the washing procedure, all solutions were filtered with hydrophilic 0.45-μm cellulose filters.

As a first approximation, one can speculate that the coating of metal nanoparticles with cationic dyes due to electrostatic interactions will generate a uniform molecular distribution on the surface, according

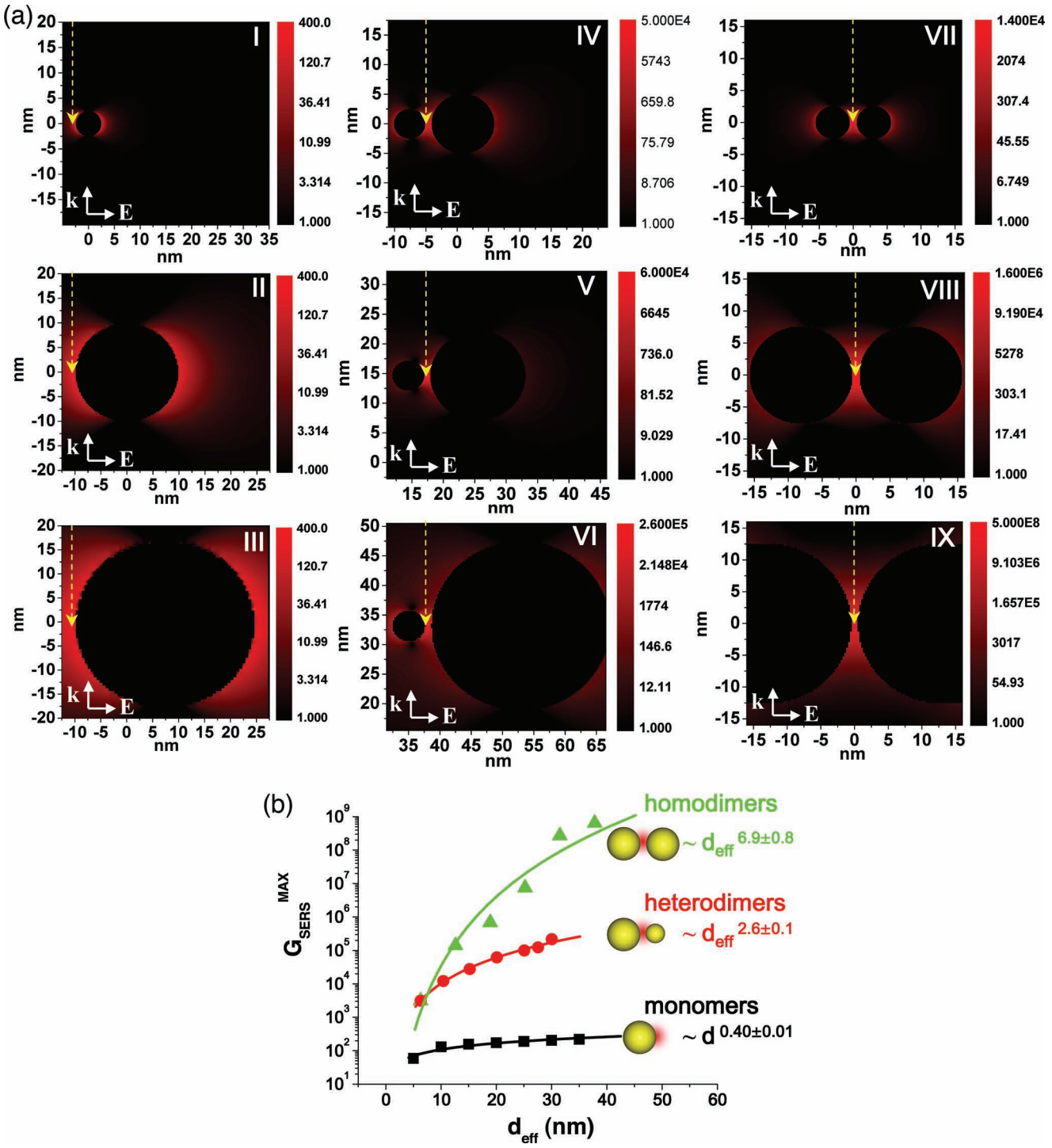

Figure 5. G_{SERS} calculations for 632.8 nm excitation. A) The plots of G_{SERS} for AuNPs monomers of 5 (I), 15 (II), and 35 (III) nm respectively, for AuNPs heterodimers of 5 and 10 (IV), 15 (V), and 27.5 (VI) nm respectively and for AuNPs homodimers of 5 (VII), 15 (VIII), and 25 (IX) nm respectively. B) G_{SERS}^{MAX} in the point of maximum amplification for a distance of 0.5 nm from the surface of AuNPs (indicated by yellow arrows in (A)) are shown for monomers (black squares), heterodimers (red circles), and homodimers (green triangles) versus the effective size of the target d_{eff} and are fitted with a power law with exponent of 0.40 ± 0.01 (black line), 2.6 ± 0.1 (red line), and 6.9 ± 0.8 (green line) respectively.

to what is usually assumed.[50,66,67] However, there may be differences in the surface distribution of different dyes because i) different dyes may have a different affinity to the AuNP surface; ii) some dyes may accumulate preferentially at the hot spots in dimers; iii) the Raman reporters can diffuse towards or outwards the hot spots on the surface of metal nanoparticles and this process may take place in a different way for different dyes.[49,68] Obtaining experimental information about the distribution of cationic dyes on AuNPs surface is a very complicated

problem, but in the present work the differences in the surface distribution of the Raman reporters are partly reduced because i) all SERS labels were obtained by the same procedure; ii) we used high concentrations of dyes, which facilitated the saturation of the AuNP surface; iii) we performed the coating of AuNPs in solution, instead of drying the solution of dyes on a substrate containing aggregated metal nanoparticles (which could facilitate accumulation of dyes at specific points during solvent evaporation); iv) we used a stabilizing PEG layer around AuNPs coated with the Raman reporters, to prevent the release of dyes from the AuNPs' surface or their migration on the surface of AuNPs.

Size selection of SERS labels was carried out by centrifugation at speeds in the 500–2000 rcf range and collecting the supernatant and the deposit as separate fractions.

Characterization of SERS Labels: SERS labels were characterized both using UV–vis spectroscopy by a Varian Cary 5 spectrometer in 2 mm optical path quartz cells, and TEM, by collecting images at 300 kV with a JEOL JEM 3010 microscope equipped with a Gatan Multiscan CCD Camera model 794. The samples for TEM analysis were prepared by evaporating AuNP suspensions on a copper grid covered with an amorphous carbon holey film.

AuNP size and concentration were evaluated by the Mie–Gans model fitting of UV–vis spectra, according to a well-consolidated procedure previously reported and by a fitting program that can be downloaded freely from the web.[69] The fitting model requires three parameters to account for spherical (Mie model) and nonspherical (Gans model) AuNPs: i) the average size of the nanoparticles (d); ii) the fraction of spherical to nonspherical gold nanoparticles; iii) the standard deviation (σ_G) of a Gaussian function used to describe the shape distribution of nonspherical nanoparticles. For AuNPs, we used the dielectric constant of gold reported by Palik and corrected for the size according to Kreibig.[69–72]

The results of the Mie–Gans fitting were confirmed by independent TEM measurements on several SERS label samples and showed an accuracy of the order of 6% when compared to TEM-measured average size, in agreement with that already reported previously for tens of AuNP solutions.[69] In our previous report, we also measured by independent inductively coupled plasma mass spectroscopy (ICP-MS) analysis that the accuracy of the Mie–Gans model for the estimation of the concentration of AuNPs in water is of the order of 4%.[42] Therefore, we exploited the Mie–Gans model to obtain the rapid determination of AuNP size and concentration over a large number of samples, without the need for TEM and ICP-MS measurements on each individual sample.

The micro-Raman measurements of SERS labels solutions were recorded by focusing the 5X objective (NA 0.12, 36% coverage) of a Renishaw InVia micro-Raman instrument (charge-coupled device; CCD detector with 100 µm slits) on the middle of a 2-mm optical path quartz cuvette and using the 632.8 nm line of a He–Ne laser with an output power of 13 mW. The Raman signal collected on an internal silicon chip was used every time to account for small (less than 5%) intensity fluctuations of the Raman spectrometer. Acquisition times of 100–300 s were used.

Calculation of $d\sigma_R/d\Omega$: The calculation of the differential Raman-scattering cross-section followed a procedure already described in the literature. The absolute differential Raman-scattering cross-section $d\sigma_R/d\Omega$ for a single scattering object is defined according to Equation 7:[1,44,73]

$$I_R(\lambda_R) = \frac{d\sigma_R}{d\Omega} I_i(\lambda_i) \delta\Omega \quad (7)$$

where $I_i(\lambda_i)$ is the incident laser power with wavelength λ_i and $I_R(\lambda_R)$ is the intensity of the Raman radiation scattered at λ_R in the solid angle $\delta\Omega$. The Raman-scattering cross-section $(d\sigma_R/d\Omega)_{Label}$ for single SERS labels can be evaluated using Equation 8:

$$\left(\frac{d\sigma_R}{d\Omega}\right)_{Label} = \frac{I_{Labels}}{C_{Labels}} \frac{C_{Standard}}{I_{Standard}} \left(\frac{d\sigma_R}{d\Omega}\right)_{Standard} \quad (8)$$

where C_{Labels} is the concentration of AuNPs constituting the SERS labels, obtained by fitting the labels UV–vis spectra with the Mie–Gans model, I_{Labels} is the intensity of Raman signals of each sample, $I_{Standard}$ is the intensity of the Raman signal of a Raman standard with known concentration $C_{Standard}$ and known Raman-scattering cross-section $(d\sigma_R/d\Omega)_{Standard}$.

Two different standards were used: 2-bromo-2-methylpropane (2B2MP, >98%, Sigma Aldrich) and dichloromethane (DM, anhydrous, >99.8%, Fluka). 2B2MP and DM have been frequently used as Raman standards.[1,44,73] 2B2MP or DM was placed in a 2 mm optical path quartz cuvette and analyzed with the same experimental conditions adopted for the SERS label solutions. The spectra of the two standards are reported in the Supporting Information. The 302 ($4.75\ 10^{-30}$ cm^2 sr^{-1}) and 516 cm^{-1} ($5.58\ 10^{-30}$ cm^2 sr^{-1}) modes of 2B2MP and the 713 cm^{-1} ($3.10\ 10^{-30}$ cm^2 sr^{-1}) mode of DM were used for obtaining absolute values of $d\sigma_R/d\Omega$. The Raman bands of standards and SERS labels were fitted with a Lorentzian curve, according to literature procedures, to obtain a more accurate comparison.[1,44,73] The $d\sigma_R/d\Omega$ value was calculated for the most intense band in the Raman spectrum of each SERS label, by comparison with the three bands of the Raman standards, therefore we obtained three values for each sample. The standard deviation on the three values of $d\sigma_R/d\Omega$ is of the order of 18% and is the dominating error source of our method, since the errors due to the quantum efficiency of the Raman spectrometer at different wavenumbers in the 300–1700 cm^{-1} range for excitation at 632.8 nm are negligible, according to the specifications provided by the producer of the instrument.

Local Electric Field Calculations: The local electric field in the proximity of AuNPs was calculated by the DDA method using the software developed by Draine and Flatau (DDSCAT 7.1 and the relative DDFIELD code).[74] We considered three different shapes (targets): i) isolated spherical nanoparticles with sizes in the 5–35 nm range; ii) dimers where one of the AuNP had a fixed size of 5 nm and the other AuNP had a size varied in the 5–35 nm range, with an interparticle gap of 1 nm (heterodimers); iii) two nanoparticles with the same size, varied in the 5–35 nm range and with an interparticle gap of 1 nm (homodimers). We used a number of dipoles varied between 600000–800000 for each target, which corresponded to a maximum interdipole spacing of 0.27 nm. For metal particles in the 2–200 nm size range, an error smaller than 10% is usually achieved by using a number of dipoles at least of the order of 10^4 and using interdipole spacing much smaller than the wavelengths of interest.[72,74,75] The refractive index of water and the size-corrected dielectric constant, as reported for the Mie–Gans fitting,[69–72] were used. We considered the incident wavelength of 632.8 nm and the electric field parallel to the axis of the dimers.

Supporting Information

Supporting Information is available from the Wiley Online Library or from the author.

Acknowledgements

The authors gratefully acknowledge Prof. S. Polizzi for support with TEM measurements and G. Marcolongo for useful discussions.

Received: July 8, 2011
Revised: September 8, 2011
Published online: November 17, 2011

[1] E. C. Le Ru, E. Blackie, M. Meyer, P. G. Etchegoin, *J. Phys. Chem. C* **2007**, *111*, 13794.
[2] S. Nie, S. R. Emory, *Science* **1997**, *275*, 1102.
[3] J. R. Lombardi, R. L. Birke, *Acc. Chem. Res.* **2009**, *42*, 734.

[4] M. Moskovits, D. P. Dilellla, *Chem. Phys. Lett.* **1980**, *73*, 500.
[5] M. Muniz-Miranda, *J. Raman Spectrosc.* **2002**, *33*, 295.
[6] F. Schedin, E. Lidorikis, A. Lombardo, V. G. Kravets, A. K. Geim, A. N. Grigorenko, K. S. Novoselov, A. C. Ferrari, *ACS Nano* **2010**, *4*, 5617.
[7] X. Qian, X. H. Peng, D. O. Ansari, Q. Yin-Goen, G. Z. Chen, D. M. Shin, L. Yang, A. N. Young, M. D. Wang, S. Nie, *Nat. Biotechnol.* **2008**, *26*, 83.
[8] S. Wachsmann-Hogiu, T. Weeks, T. Huser, *Curr. Opin. Biotechnol.* **2009**, *20*, 63.
[9] A. Shen, L. Chen, W. Xie, J. Hu, A. Zeng, R. Richards, J. Hu, *Adv. Funct. Mater.* **2010**, *20*, 969.
[10] C. L. Zavaleta, B. R. Smith, I. Walton, W. Doering, G. Davis, B. Shojaei, M. J. Natan, S. S. Gambhir, *Proc. Natl. Acad. Sci. USA* **2009**, *106*, 13511–13516.
[11] L. Wang, M. B. O'Donoghue, W. Tan, *Nanomedicine* **2006**, *1*, 413.
[12] D. K. Lim, K. S. Jeon, H. M. Kim, J. M. Nam, Y. D. Suh, *Nat. Mater.* **2009**, *9*, 60.
[13] D. C. Kennedy, K. A. Hoop, L. L. Tay, J. P. Pezacki, *Nanoscale* **2010**, *2*, 1413.
[14] B. H. Jun, M. S. Noh, J. Kim, G. Kim, H. Kang, M. S. Kim, Y. T. Seo, J. Baek, J. H. Kim, J. Park, *Small* **2009**, *6*, 119.
[15] Y. Huang, V. P. Swarup, S. W. Bishnoi, *Nano Lett.* **2009**, *9*, 2914.
[16] S. D. Hudson, G. Chumanov, *Anal. Bioanal. Chem.* **2009**, *394*, 679.
[17] D. Graham, K. Faulds, *Chem. Soc. Rev.* **2008**, *37*, 1042.
[18] L. Fabris, M. Dante, T. Q. Nguyen, J. B. H. Tok, G. C. Bazan, *Adv. Funct. Mater.* **2008**, *18*, 2518.
[19] Y. C. Cao, R. Jin, C. A. Mirkin, *Science* **2002**, *297*, 1536.
[20] L. Sun, K. B. Sung, C. Dentinger, B. Lutz, L. Nguyen, J. Zhang, H. Qin, M. Yamakawa, M. Cao, Y. Lu, A. J. Chmura, J. Zhu, X. Su, A. A. Berlin, S. Chan, B. Knudsen, *Nano Lett.* **2007**, *7*, 351.
[21] W. E. Doering, M. E. Piotti, M. J. Natan, R. G. Freeman, *Adv. Mater.* **2007**, *19*, 3100.
[22] E. S. Allgeyer, A. Pongan, M. Browne, M. D. Mason, *Nano Lett.* **2009**, *9*, 4784.
[23] X. Su, J. Zhang, L. Sun, T. W. Koo, S. Chan, N. Sundararajan, M. Yamakawa, A. A. Berlin, *Nano Lett.* **2005**, *5*, 49.
[24] X. M. Qian, S. M. Nie, *Chem. Soc. Rev.* **2008**, *37*, 912.
[25] M. A. Dobrovolskaia, S. E. McNeil, *Nat. Nanotech.* **2007**, *2*, 469.
[26] Y. C. Cao, R. Jin, J. M. Nam, C. S. Thaxton, C. A. Mirkin, *J. Am. Chem. Soc.* **2003**, *125*, 14676.
[27] C. Fernández-López, C. Mateo-Mateo, R. A. Álvarez-Puebla, J. Pérez-Juste, I. Pastoriza-Santos, L. M. Liz-Marzán, *Langmuir* **2009**, *25*, 13894.
[28] B. Kustner, M. Gellner, M. Schutz, F. Schoppler, A. Marx, P. Strobel, P. Adam, C. Schmuck, S. Schlucker, *Angew. Chem. Int. Ed.* **2009**, *48*, 1950.
[29] M. Y. Sha, H. Xu, M. J. Natan, R. Cromer, *J. Am. Chem. Soc.* **2008**, *130*, 17214.
[30] S. Lee, S. Kim, J. Choo, S. Y. Shin, Y. H. Lee, H. Y. Choi, S. Ha, K. Kang, C. H. Ohs, *Anal. Chem.* **2007**, *79*, 916.
[31] G. von Maltzahn, A. Centrone, J. H. Park, R. Ramanathan, M. J. Sailor, T. A. Hatton, S. N. Bhatia, *Adv. Mater.* **2009**, *21*, 3175.
[32] W. Li, P. H. C. Camargo, X. Lu, Y. Xia, *Nano Lett.* **2009**, *9*, 485.
[33] J. Xie, Q. Zhang, J. Y. Lee, D. I. C. Wang, *ACS Nano* **2008**, *2*, 2473.
[34] M. Sanles-Sobrido, W. Exner, L. Rodrìguez-Lorenzo, B. Rodrìguez-Gonzaìez, M. Correa-Duarte, R. A. Aìlvarez-Puebla, L. M. Liz-Marzán, *J. Am. Chem. Soc.* **2009**, *131*, 2699.
[35] F. McKenzie, K. Faulds, D. Graham, *Nanoscale* **2010**, *2*, 78.
[36] R. Wilson, A. R. Cossins, D. G. Spiller, *Angew. Chem. Int. Ed.* **2006**, *45*, 6104.
[37] G. Goddard, L. O. Brown, R. Habbersett, C. I. Brady, J. C. Martin, S. W. Graves, J. P. Freyer, S. K. Doorn, *J. Am. Chem. Soc.* **2010**, *132*, 6081.
[38] V. Amendola, M. Meneghetti, *Phys. Chem. Chem. Phys.* **2009**, *11*, 3805.
[39] H. Muto, K. Yamada, K. Miyajima, F. Mafune, *J. Phys. Chem. C* **2007**, *111*, 17221.
[40] C. G. Blatchford, J. R. Campbell, J. A. Creighton, *Surf. Sci.* **1982**, *120*, 435.
[41] P. Galletto, P. F. Brevet, H. H. Girault, R. Antoine, M. Broyer, *J. Phys. Chem. B* **1999**, *103*, 8706.
[42] V. Amendola, M. Meneghetti, S. Fiameni, S. Polizzi, G. Fracasso, A. Boscaini, M. Colombatti, *Anal. Methods* **2011**, *3*, 849.
[43] U. Resch-Genger, M. Grabolle, S. Cavaliere-Jaricot, R. Nitschke, T. Nann, *Nat. Methods* **2008**, *5*, 763.
[44] S. Shim, C. M. Stuart, R. A. Mathies, *ChemPhysChem.* **2008**, *9*, 697.
[45] A. Mohammed, H. Ågren, P. Norman, *Phys. Chem. Chem. Phys.* **2009**, *11*, 4539.
[46] A. Mohammed, H. Ågren, P. Norman, *Chem. Phys. Lett.* **2009**, *468*, 119.
[47] A. B. Myers, *Acc. Chem. Res.* **1997**, *30*, 519.
[48] L. Jensen, L. L. Zhao, J. Autschbach, G. C. Schatz, *J. Chem. Phys.* **2005**, *123*, 174110.
[49] E. C. Le Ru, P. G. Etchegoin, M. Meyer, *J. Chem. Phys.* **2006**, *125*, 204701.
[50] P. G. Etchegoin, M. Meyer, E. Blackie, E. C. Le Ru, *Anal. Chem.* **2007**, *79*, 8411.
[51] Y. Fang, N. H. Seong, D. D. Dlott, *Science* **2008**, *321*, 388.
[52] E. C. Le Ru, P. G. Etchegoin, *J. Chem. Phys.* **2009**, *130*, 181101.
[53] E. C. Le Ru, P. G. Etchegoin, *Chem. Phys. Lett.* **2006**, *423*, 63.
[54] E. C. Le Ru, M. Meyer, E. Blackie, P. G. Etchegoin, *J. Raman Spectrosc.* **2008**, *39*, 1127.
[55] A. Lee, G. F. S. Andrade, A. Ahmed, M. L. Souza, N. Coombs, E. Tumarkin, K. Liu, R. Gordon, A. G. Brolo, E. Kumacheva, *J. Am. Chem. Soc.* **2011**, *133*, 7563.
[56] J. Margueritat, H. Gehan, J. Grand, G. Levi, J. Aubard, N. Felidj, A. Bouhelier, G. Colas-Des-Francs, L. Markey, M. D. Lucas, A. Dereux, E. Finot, *ACS Nano* **2011**, *5*, 1630.
[57] S. E. J. Bell, M. R. McCourt, *Phys. Chem. Chem. Phys.* **2009**, *11*, 7455.
[58] S. C. Boca, C. Farcau, S. Astilean, *Nucl. Instr. Meth. Phys. Res.* **2009**, *267*, 406.
[59] G. B. Braun, S. J. Lee, T. Laurence, N. Fera, L. Fabris, G. C. Bazan, M. Moskovits, N. O. Reich, *J. Phys. Chem. C* **2009**, *113*, 13622.
[60] M. Futamata, Y. Yu, T. Yajima, *J. Phys. Chem. C* **2011**, *115*, 5271.
[61] H. Guo, F. Ruan, L. Lu, J. Hu, J. Pan, Z. Yang, B. Ren, *J Phys. Chem. C* **2009**, *113*, 10459.
[62] G. Grasso, L. D'Urso, E. Messina, F. Cataldo, O. Puglisi, G. Spoto, G. Compagnini, *Carbon* **2009**, *47*, 2611.
[63] S. Pal, L. E. Depero, I. Alessandri, *Nanotechnology* **2010**, *21*, 425701.
[64] E. Hao, G. C. Schatz, *J. Chem. Phys.* **2004**, *120*, 357.
[65] K. Li, M. I. Stockman, D. J. Bergman, *Phys. Rev. Lett.* **2003**, *91*, 227402.
[66] J. C. Jones, C. McLaughlin, D. Littlejohn, D. A. Sadler, D. Graham, W. E. Smith, *Anal. Chem.* **1999**, *71*, 596.
[67] R. Tantra, R. J. C. Brown, M. J. T. Milton, *J. Raman Spectrosc.* **2007**, *38*, 1469.
[68] Y. Kitahama, Y. Tanaka, T. Itoh, Y. Ozaki, *Phys. Chem. Chem. Phys.* **2010**, *12*, 7457.
[69] V. Amendola, M. Meneghetti, *J. Phys. Chem. C* **2009**, *113*, 4277.
[70] E. D. Palik, *Handbook of Optical Constants of Solids*, Academic Press **1985**.
[71] U. Kreibig, M. Vollmer, *Optical Properties of Metal Clusters*, Springer, Berlin **1995**.
[72] V. Amendola, O. M. Bakr, F. Stellacci, *Plasmonics* **2010**, *5*, 85.
[73] M. J. Colles, J. E. Griffiths, *J. Chem. Phys.* **1972**, *56*, 3384.
[74] B. T. Draine, P. J. Flatau, *J. Opt. Soc. Am. A* **1994**, *11*, 1491.
[75] C. Noguez, *J. Phys. Chem. C* **2007**, *111*, 3806.